Fibers and Polymers 2020, Vol.21, No.1, 33-44
DOI 10.1007/s12221-020-9402-1

ISSN 1229-9197 (print version)
ISSN 1875-0052 (electronic version)

Design of Novel 3D-Scaffold as a Potential Material to Induct Epidermal-Dermal Keratinocytes of Human-Adipose-Derived Stem Cells and Promote Fibroblast Cells Proliferation for Skin Regeneration

Azadeh Izadyari Aghmiuni[1], Mazyar Sharifzadeh Baei[1]*, Saeed Heidari Keshel[2], and Azim Akbarzadeh Khiyavi[3]

[1]*Department of Chemical Engineering, Ayatollah Amoli Branch, Islamic Azad University, Amol 678, Iran*
[2]*Department of Tissue Engineering and Applied Cell Science, Shahid Beheshti University of Medical Sciences, Tehran 19839-63113, Iran*
[3]*Department of Nanobiotechnology, Pasteur Institute of Iran, Tehran 1316943551, Iran*
(Received April 24, 2019; Revised July 14, 2019; Accepted July 17, 2019)

Abstract: Dermal lesions and chronic wounds associated with burns or some diseases like diabetes are the more important public health concerns which can affect the quality of life. Currently, tissue engineering is considered as the most effective therapeutic method although the design of polymeric substrates for epidermal-dermal differentiation and wound healing (scar-free) is the main challenge. For this purpose, we designed a hybrid three-dimensional scaffold (CPCP) based on collagen/chitosan modified by PEG/PCL composite that can imitate differentiation pattern of both epidermis/dermis cells, via mimicking the structure and function of human skin. The physicochemical, mechanical and biological properties of designed scaffolds were evaluated to study their function for skin tissue engineering applications. Comparison of FTIR analysis showed a chemical similarity between CPCP and decellularized dermal matrix (DDM). Our results showed that combination of two natural/two synthetic polymers led to the formation of stronger 3D-network together with higher modulus (~18), water absorption (4-fold), porosity (~92) and consequently lower pores size (~54 μm), compared to natural, synthetic and natural/ synthetic copolymer-based scaffolds. The observation of human skin fibroblast cells proliferation and morphology showed that CPCP was more beneficial to cell adhesion, proliferation, and extension than that of other designed scaffolds due to its hydrophilicity and higher wettability (WCA=60 °). According to the results of RT-PCR, the more expression of epidermal-dermal keratinocytes induced by human-adipose-derived stem cells was observed on the CPCP along with a pattern similar to skin. The results demonstrate CPCP can act as a super-absorbent substrate/dressing for continuous absorption of wound exudates. Furthermore, it can potentially be effective for re-epithelialization of skin together with its derivative (hair follicles, sebaceous/sweat glands). This study indicates new insights into the design of skin- engineered scaffolds.

Keywords: Wound healing, Skin tissue engineering, Natural polymer, Epidermal-dermal keratinocytes, Extracellular matrix (ECM) structure

Introduction

The skin as an external cover of the body plays an important role in the protection of internal organs [1,2]. Hence, the initial treatment of dermal injuries such as burns, venous leg ulcer, and other chronic wounds is essential to prevent or reduce the spread of infections in the body. In the past decades, the xenografts, allografts, and autografts were widely used for wound healing. Although, the major problems associated with these therapeutic methods were the limitation of donor sites, antigenicity, and immunogenicity [3,4].

Nowadays, studies reveal that skin tissue engineering as a new approach can be effective to overcome the mentioned problems [5-7]. This method includes the use of polymers and design of porous scaffolds to promote cells adhesion, proliferation and differentiation and consequently the formation of new tissue or improvement of biological tissue [7,8].

However, the crucial challenge in skin tissue engineering is the design of a dermal-like scaffold that can mimic the structure and biomechanical and physicochemical functions of the normal skin to regenerate both main layers of the epidermis (keratinocytes) and dermis (hair follicle and sweat/sebaceous glands etc.). Thus, the understanding the chemical structure and biological behavior of polymers as materials of scaffold constructor can lead to the more accurate design of scaffold along with better interactions of cell- cell (to form epidermis) and cell-scaffold (to form dermis) which results in the scar-free skin regeneration [9,10].

In this field, hyaluronic acid and chitosan are the most famous natural polymers that provide the proper conditions for cell-cell interactions, due to the presence of hydrophilic groups in their chemical structure [5,11,12]. Nevertheless, chitosan as a marine polysaccharide and biomaterial of nontoxic, antibacterial and low-cost has been developed in a wide range of clinical researches and tissue engineering applications [13-17]. Collagen is another natural polymer (biomaterial) that applied in skin engineered scaffolds structure due to protein-based fibers that can create a porous network similar to the mesh-like fibrillar structure of the dermal extracellular matrix (ECM) [5,18]. However, a single-polymer scaffold such as collagen or chitosan scaffolds

*Corresponding author: chemengineer.phd86@gmail.com

alone cannot provide an appropriate physical structure for the regulation of cellular behaviors (adhesion, proliferation and differentiation) [19,20]. Hence, the combination of two and more polymers has been suggested as an efficient method for scaffolds design [21-24]. This can also provide the more stable structure compared to the mentioned single-polymer scaffolds and promote cells adhesion, proliferation and differentiation on composite substrates like collagen/chitosan scaffolds because of bonding proteoglycans of collagen with chitosan chains [13,15].

Although collagen/chitosan scaffolds as natural composites provide the biophysical structure similar to skin, however, the fast degradation and the poor mechanical properties of these scaffolds are considered as the limitations of natural polymer-based composite scaffolds.

The studies have shown that synthetic polymers can improve the mechanical and physicochemical characteristics of the natural scaffolds [25-27]. Moreover, the combination of natural and synthetic polymers covers poor hydrophilicity of synthetic materials and lead to the balance of water absorption, surface modification, and better interactions between cell and scaffold. However, the selection of the suitable polymer plays an important role in biological and biomechanical behavior similarity of the scaffold to normal skin for mimicking cell growth pattern [28].

Polyethylene glycol (PEG) is one of the most popular options that led to an increase in cell adhesion and promotion of cell signaling, due to the better interaction with the polysaccharide or peptide chains [26,29].

Furthermore, poly(ε-caprolactone) (PCL) as the most famous synthetic polymers can increase not only mechanical strength of scaffold due to integrity chemical structure and miscibility with biopolymers but also improve the penetration of cells into the scaffold due to the existence of sites of cell recognition [26,30,31].

Although, various constructs exist in this field, and the skin tissue-engineered scaffolds for various wounds healing have notably evolved in recent years. However, the design of new scaffolds has continued to achieve ideal substitutes that can regenerate skin together with its derivative appendages, like keratinocytes, hair follicles, sebaceous glands, and sweat glands. Based on the reports, three dimensional (3D) scaffolds due to higher porosity and the regular supply of oxygen and nutrients provide a better architecture for cellular adhesion, migration, proliferation, and differentiation and consequently the acceleration of wound healing process, compared to two dimensional (2D) films [32]. It seems that such scaffolds can imitate not only the internal architecture of the ECM but also provide the chemical, structural and mechanical properties similar to the skin for fibroblasts proliferation and epidermal-dermal keratinocytes differentiation.

Therefore, the primary goal of this study is to fabricate hybrid 3D scaffold comprises both polymers of natural and synthetic to develop substitutes similar to normal human skin that can lead to epidermis and dermis cells differentiation and proliferation. For this purpose, chitosan was selected due to the chemical structure similar to the glycosaminoglycans (GAGs) of skin. To optimize the biological properties of the scaffold, collagen was added to the chitosan solution. PEG-PCL composite was also used to modify the physicochemical and mechanical properties of the hybrid scaffold. The freeze-drying method suggested for the creation of the more homogenous 3D structure that results in smaller pores, due to faster ice crystals removal via sublimation process [33]. In followed by, physicochemical and mechanical characteristics of the novel hybrid scaffold were evaluated and compared to synthetic, natural polymer-based scaffolds and decellularized dermal-based matrix. Finally, we assessed human skin fibroblast (HSF) cell viability ability and differentiation potential of human adipose-derived stem cells (h-ASCs) on all scaffolds and provided evidence that designed 3D micro-porous scaffold consisting of two natural and two synthetic polymers can promote not only HSF and h-ASCs growth but also can lead to the switch from proliferation to differentiation. To our knowledge, it is the first time that a hybrid 3D scaffold fabricated from polymers inspired by the macromolecular-based components of dermal-ECM (as a specific induction substrate), can induce both dermis and epidermis cells by h-ASCs differentiation, in the absence of growth factors. It is notable that, h-ASCs were selected due to ease of isolation from human tissues and less ethical problems in medical researches [34-37].

Experimental

Materials

Bovine collagen solution (Acid-soluble collagen; Type I), chitosan (Mn: 234 kDa, deacetylation degree of 95 %), poly-ε-caprolactone (PCL, Mn: 45000), polyethylene glycol (PEG, Mn: 6000), N-hydroxysuccinimide (NHS), 1-Ethyl-3-[3-dimethylaminopropyl] carbodiimide hydrochloride (EDC), Acetic Acid (glacial), tetrazolium salt 3-(4, 5-dimethylthiazol-2-yl)-2,5-diphenyltetrazolium bromide (MTT) and dimethyl sulfoxide (DMSO) were obtained from Sigma-Aldrich (USA). Dulbecco's modified eagle medium (DMEM), penicillin-streptomycin, and fetal bovine serum (FBS) were also obtained from Gibco (USA).

Preparation of PEG/Chi Solution

Initially, 1 g of PEG and chitosan were dissolved in 10 and 20 m*l* of dH_2O (deionized water) and acetic acid (0.5 M) respectively, at 25 ^oC for 24 h. Then, the cross-linking solution of NHS at a weight ratio of 10 (wt%) was added to PEG polymeric solution and mixed (on the stirrer) for 1 h. Afterward, the 10 m*l* of chitosan gel was slowly added to 7.5 m*l* of the mentioned solution and mixed on the stirrer, for an additional 12 h.

Table 1. Composition of designed scaffolds

Scaffolds code	Collagen volume ratio	PEG/Chitosan volume ratio	PCL volume ratio
CPCP	0.13	1.5:2	1
PCP	0	1.5:2	1
CC	0.13	0:2	0
PEPC	0	1.5:0	1

Preparation of PCL Solution

PCL solution was prepared by dissolving 1 g of PCL powder in 70 % acetic acid (33.33 m*l*) at 50 °C for 24 h. Then, the EDC cross-linker with 20 wt% was added to this solution and mixed at 25 °C for 1 h.

Preparation of Ternary Solution

To prepare PEG/Chi/PCL (PCP) solution, 5 m*l* of PCL solution was added drop-wise (for 5 mins) to PEG/Chi copolymer, with slow stirring. Then, the PCP solution was mixed overnight at 25 °C.

Preparation of Collagen/PEG/Chi/PCL Scaffold

The collagen/PEG/Chi/PCL (CPCP) composite solution was prepared by adding 675 μ*l* of collagen solution to 22.5 m*l* of PCP solution. Moreover, collagen/chitosan (CC) and PEG/PCL (PEPC) solutions were prepared to assess the role of natural and synthetic polymers in mimicry of skin ECM structure and functions (Table 1). It is notable that the pH changes are the main factor for crosslinking collagen and chitosan.

Afterward, 2 m*l* of the solutions were separately cast into each well of 24-well tissue culture plates (Sigma-Aldrich, USA). Then, the plates were frozen at -20 °C for 12 h and -80 °C for 24 h, respectively. Finally, samples were transferred to a freeze-dryer (Gamma 2-16 LSC, Martin Christ, Germany) and dried by lyophilization (freeze-drying) at -80 °C, for 48 h to prepare composite scaffolds. The scaffolds were stored at 4 °C, to assess in vitro assays (physicochemical, mechanical and biological properties) and study their suitability to be used as wound dressing or substrate of epidermal differentiation.

Characterization of 3D Scaffolds

Surface Chemistry Analysis

The final composition of the lyophilized scaffolds was determined by FTIR-spectrum analysis (Fourier Transform Infrared Spectroscopy, Model-ALPHA, Bruker, Germany). The scaffolds' spectra were acquired from 400-4000 cm^{-1} with 4 cm^{-1} resolution and an average of 16 scans.

Mechanical Behavior

A tensile test was performed to determine the mechanical properties of the scaffolds. Accordingly, tensile strength, elastic modulus and elongation at break point were measured using a tensile tester instrument (Zwick/Roell, 1446) at a strain rate of 2 mm/min, and the ASTM D3039 standard guide for testing polymer matrix composite materials [38].

Wettability

Wettability of scaffolds and water contact angle (WCA) on surfaces were determined by a semi-automatic device-contact angle goniometer (CAG-10, JIKAN), at 25 °C. Distilled water was selected as a reference fluid and droplets of 2 μ*l* were placed on the surface of scaffolds. Wettability process was recorded using a digital camera.

Swelling

The scaffolds swelling assay was carried out by immersing the dried scaffolds in PBS (pH=7.4), at 37 °C and predetermined time intervals (i.e., 1, 3, 5, 10, 24, and 48 h). The weight of scaffolds before and after immersion in PBS was recorded as the weight of dry and wet scaffold. Then, the percentage of scaffolds swelling was determined through equation (1) [39,40].

$$\text{Swelling } \% = \frac{W_w - W_d}{W_d} \times 100 \quad (1)$$

W_d: initial dry weight of the scaffolds

W_w: after removing the excess scaffolds water with filter paper

Enzymatic Degradation

The degradation profile of the scaffolds was determined according to a previous method [40]. In brief, dried scaffolds with the weight of W_d were immersed in PBS containing 13 mg/*l* lysozyme (Sigma, USA) (enzymatic concentration similar to human blood serum), at 37 °C and regular time (2, 4, 8, and 14 days). At the end of each period, the scaffolds were removed from the degradation medium and weighed, after completely dried (W_t). The degradation percentage of scaffolds at each time point was obtained by equation (2).

$$\text{Degradation } \% = \frac{W_d - W_t}{W_d} \times 100 \quad (2)$$

Porosity

The porosity of the composite scaffolds was measured by a liquid displacement method [41]. Briefly, dried scaffolds of each group were first weighed (W_d) then immersed in absolute ethanol (1 h) and reweighed (W_w). The porosity was determined with equation (3). Three scaffolds for each group were used to measure the average value along with SD.

$$\text{Porosity } \% = \frac{W_w - W_d}{D_e \times V_s} \times 100 \quad (3)$$

D_e: density of the ethanol at 25 °C

V_s: the volume of the swollen scaffold

Finally, the morphology and inner structure of scaffolds were analyzed using a scanning electron microscope (SEM, XL30 ESEM, Philips, Germany), at an accelerating voltage of 20 kV. The morphology and pores size of scaffolds were assessed by Clemex vision software 3.5. At least 50 measurements at each SEM image were tested to assess

mean and standard deviation of pores size.

Biological Properties of Scaffolds

The assessment of cell behavior (adhesion, proliferation, and viability) was carried out to test scaffolds biocompatibility and biological efficiency. Prior to cell seeding, scaffolds were sterilized by ultraviolet (UV rays, 254 nm wavelength, 2 h) and placed into 96-well plates. Afterward, HSF cells (Human Skin Fibroblast, NCBI Code: C192, Iranian Pasture Institute cell bank, Tehran, Iran) were seeded onto the scaffolds (at a density of 1×10^6 cells per well, according to the size and type of 3D scaffold) and culture medium contains DMEM-low glucose, 15 % FBS, and penicillin (100 U/m*l*)/streptomycin (1000 U/m*l*), added to each well-containing cell-scaffold. After 5 h of incubation, scaffolds were washed with PBS (3 times) and cells were fixed with 2.5 wt% glutaraldehyde solution. After 30 min, the scaffolds were washed again with PBS and post-fixation was performed with 1 % Osmium tetroxide. Finally, the scaffolds were dried, and observed under SEM (an accelerating voltage of 10.0 kV) to evaluate initial adhesion.

Moreover, the plates were incubated at 37 °C (5 % CO_2, humidified atmosphere) for 24, 48, and 72 h, to assess cellular proliferation. Followed by, an MTT assay was performed to study the cell viability on the scaffolds. Briefly, the medium of each well was removed and replaced with 100 μ*l* of fresh medium and 20 μ*l* of MTT solution. After incubation for 4 h, MTT medium was removed, and cells were solubilized in 100 μ*l* of DMSO. Then, the absorbance of each sample was determined at a wavelength of 570 nm. The culture medium (without scaffolds) was selected as the control group (100 % cell viability). The cell viability (%) was estimated by equation (4). It is notable that, inverted microscope images were observed to evaluate cell growth on the porous scaffolds, after 72 h.

Furthermore, human eyelid adipose-derived stem cells (h-ASCs) were seeded onto the designed scaffolds at a density of 1×10^6 (cells/well) to assess differentiation potential of h-ASCs and expression level of keratinocytes induced by the mentioned cell, on the scaffolds. The 3rd passage of cells isolated in our previous study were used in this research [42].

$$\text{Cell viability (\%)} = \frac{OD_{sample}}{OD_{control}} \times 100 \quad (4)$$

OD: optical density is proportional to the mass in the cell suspension (at the wavelength of interest).

Gene Expression Analysis by Real-time PCR

The analysis of RT-PCR was carried out to assess the expression of keratinocyte-specific genes at days 7 and 14 of the h-ASCs differentiation, according to the standard protocol [43]. RNA extraction kit (TAKARA, Tokyo, Japan) was used for isolation of total RNA from cells placed on the scaffolds. Followed by, for digestion and removal of genomic DNA from extracted RNA, a DNase I treatment (TAKARA, Tokyo, Japan) was performed and the quantity of isolated RNA was evaluated using spectrophotometry (NanoDrop; Thermo, Wilmington, USA). Moreover, standard reverse transcription (RT) reactions were performed with 2 μg total RNA using RevertAid First Strand cDNA Synthesis Kit (TAKARA, Tokyo, Japan). Extracted RNA from the human normal skin cell line (C192, Iranian Pasture Institute cell bank) was also applied as a positive control.

The RT-PCR (Rotor-Gene Q Real-Time PCR System, Qiagen, USA) reaction was carried out with *SYBRR Premix Ex Taq*™ (Takara BIO, INK, Japan) that uses Taq Fast DNA Polymerase, SYBR Green I dye to detect double-stranded DNA. The gene expression levels were obtained using the $2^{-\Delta\Delta Ct}$ method (normalized against human β-actin (ACTB) as a housekeeping gene) and statistical analysis were performed using ANOVA (p-value < 0.05). The gene-specific primers were used as below: β-actin (ACTB, NM001101.4), forward: 5′-GGCGCCCTATAAAACCCAGC and reverse: 5′-GCTCGATGGGGTACTTCAGG (T_m: 60 °C); keratinocyte14 (K14, NM000526.4), forward: 5′-AGACCAAAGGTCGCT ACTGC and reverse: 5′-ATCGTGCACATCCATGACCT (T_m: 60 °C); keratinocyte10 (K10, NM000421.3), forward: 5′-ACTACTCTTCCTCCCGCAGT and reverse: 5′-CAGAGC TCCCACGGCTAAAA (T_m: 60 °C); keratinocyte18 (K18, NM000224.2), forward: AAGCCTGAGTCCTGTCCTTTCT and reverse: AGGCTTTGCATGGTCTCCTT (T_m: 61 °C).

Statistical Analysis

All tests were performed in triplicate and the results were expressed as mean±standard deviation (SD). The differences between scaffolds were evaluated with the Dunnett (2-sided) and LSD in IBM SPSS Statistics 24 software. P-values of <0.05 and <0.001 were considered as the significance level.

Results and Discussion

The chemical analysis of skin tissue-engineered scaffolds plays an important role in the description of polymers interactions and surface behaviors. The scaffold that mimics the chemical structure of skin can provide an environment with physical, mechanical and biological properties similar to epidermis or dermis [44,45].

FTIR spectra of the 3D scaffolds were shown in Figure 1. The analysis spectra indicated that the addition of chitosan into the PEPC composite to make PCP scaffold was led to a decrease in intensity of C=O and -OH peaks and shift of 1279.99 cm^{-1} to 1282.02 cm^{-1}. It could confirm the presence of amide I and III groups of chitosan and their interaction with PEPC chains, as well as enhancement of the hydrophilic groups. The CPCP spectrum also showed incorporation of collagen and PCP hybrid copolymer was led to an increase in the intensity of the -OH, amide I (C=O), amide III and

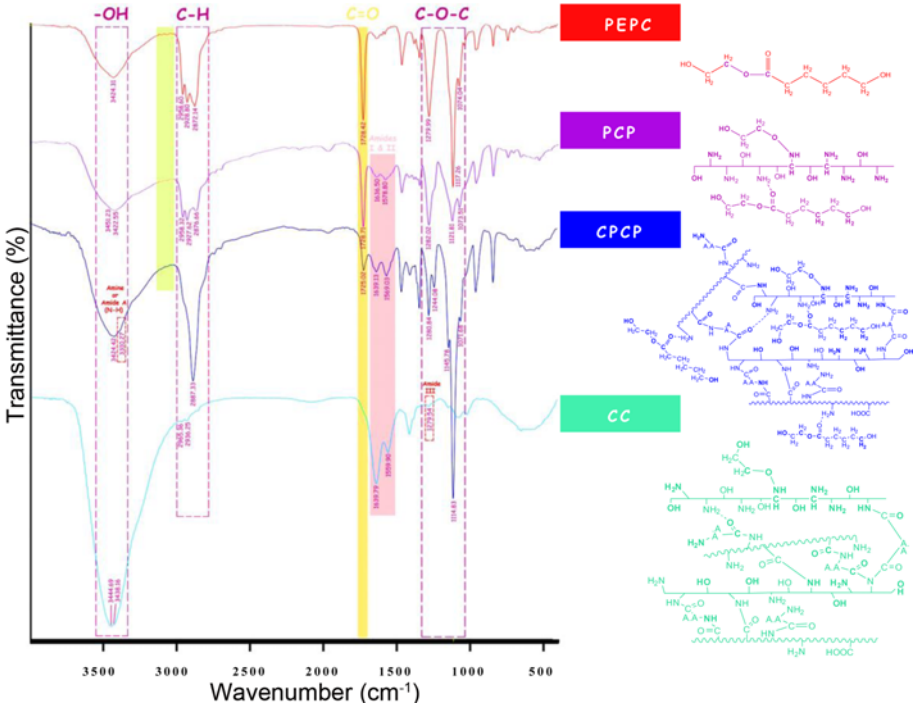

Figure 1. FTIR spectra for designed scaffolds.

amine (C-N) peaks, compared to PCP. Furthermore, mini-peaks in the range of 3000-3400 cm^{-1} that observed in PCP and PEPC spectra were removed in the CPCP spectrum due to intermolecular interactions between collagen with synthetic polymers (green range). Likewise, a weak peak at 3310.27 cm^{-1}, a single-peak at 2887.33 cm^{-1} along with a strong peak at 1114.83 cm^{-1} were appeared in CPCP spectrum, associated with N-H functional groups of amide A or amine, amide B group and interaction of amide I, II and C-O-C groups, respectively, that could be due to the formation of hydrogen bonds between chitosan and α-helix structure of collagen [46].

As a result, irrespective from skin location in the body (forearm, ear, hand, etc.), the comparison of the FTIR spectrum of scaffolds designed in this study and human epidermis in other studies [47-50] illustrated that mixture of natural and synthetic polymers was led to the formation of various bands and creation of the skin-like chemical structure (Table 2).

Mechanical Behavior Analysis

The tensile strength test was carried out to assess the elasticity and mechanical stability of scaffolds. The average of stress-strain curves and values of elastic modulus, tensile

Table 2. Absorption bands observed in the scaffolds and human epidermis

Wavenumber (cm^{-1})	Tentative assignment	Studied groups					
		PEPC	PCP	CPCP	CC	Epidermis	Ref
3400-4000	OH, NH	×	×	×	×	×	[47,48]
3000-3200	Amide A, N-H of proteins (amine) (red rectangles in Figure 1)	-	-	×	-	×	
2800-3000	C-H	×	×	×	×	×	
1670-1780	C=O of esters or phospholipids (orange range in Figure 1)	×	×	×	-	×	
1600-1650	Amide I band, proteins (pink range in Figure 1)	-	×	×	×	×	
1550-1580	Amide II	-	×	×	×	×	
1250-1280	Amide III	-	×	×	×	×	
1000-1290	C-O-C	×	×	×	-	×	

strength, and elongation at break for each scaffold are shown in Figure 2(a-e) and Table 3.

Comparison of stress-strain curves indicates that the smallest elongation-to-break was related to the binary scaffold of CC due to poor mechanical properties of natural polymers (Figure 2(e)). The same result was observed in elastic modulus for PEPC scaffold ($p<0.001$). It could be due to an increase in stiffness and lack of the hydrophilic groups in the scaffold structure. While there was no significant difference between CC and PEPC scaffolds in terms of tensile strength value that could be due to the stiffness of PCL and intramolecular forces of collagen ($p>0.001$). Nevertheless, mechanical characteristics of the mentioned scaffolds were significantly enhanced when were combined with each other. So, the tensile strength of PCP scaffold was showed an increase of ~63 % and 70 % compared to the PEPC and CC scaffolds, respectively (Table 3). Moreover, the addition of collagen (3 % total polymer weight) significantly improved CPCP mechanical properties compared to other scaffolds. This can be due to a large number of intermolecular forces that led to the formation of a stronger 3D-network (Figure 2(e) and Table 3, $p<0.001$). So that, modulus, tensile strength and elongation-at-break of CPCP were 3.5-fold, ~3-fold and 2-fold the higher than PCP scaffold, respectively; because of the formation of hydrogen bonds between the hydroxyl (-OH) groups of hydroxyproline in collagen and -OH and NH_2 groups in PEG and chitosan, as well as increase of $-CH_3$ side groups. It was also found that little increase in force was led to deformation and consequently the creation of a toe region for CPCP and CC scaffolds. This region was related to the straightening of the wavy collagen fibers (Figure 2(a) and (c)). These results corresponded with mechanical properties of a decellularized dermal matrix (DDM) in the same study and indicated that there is no

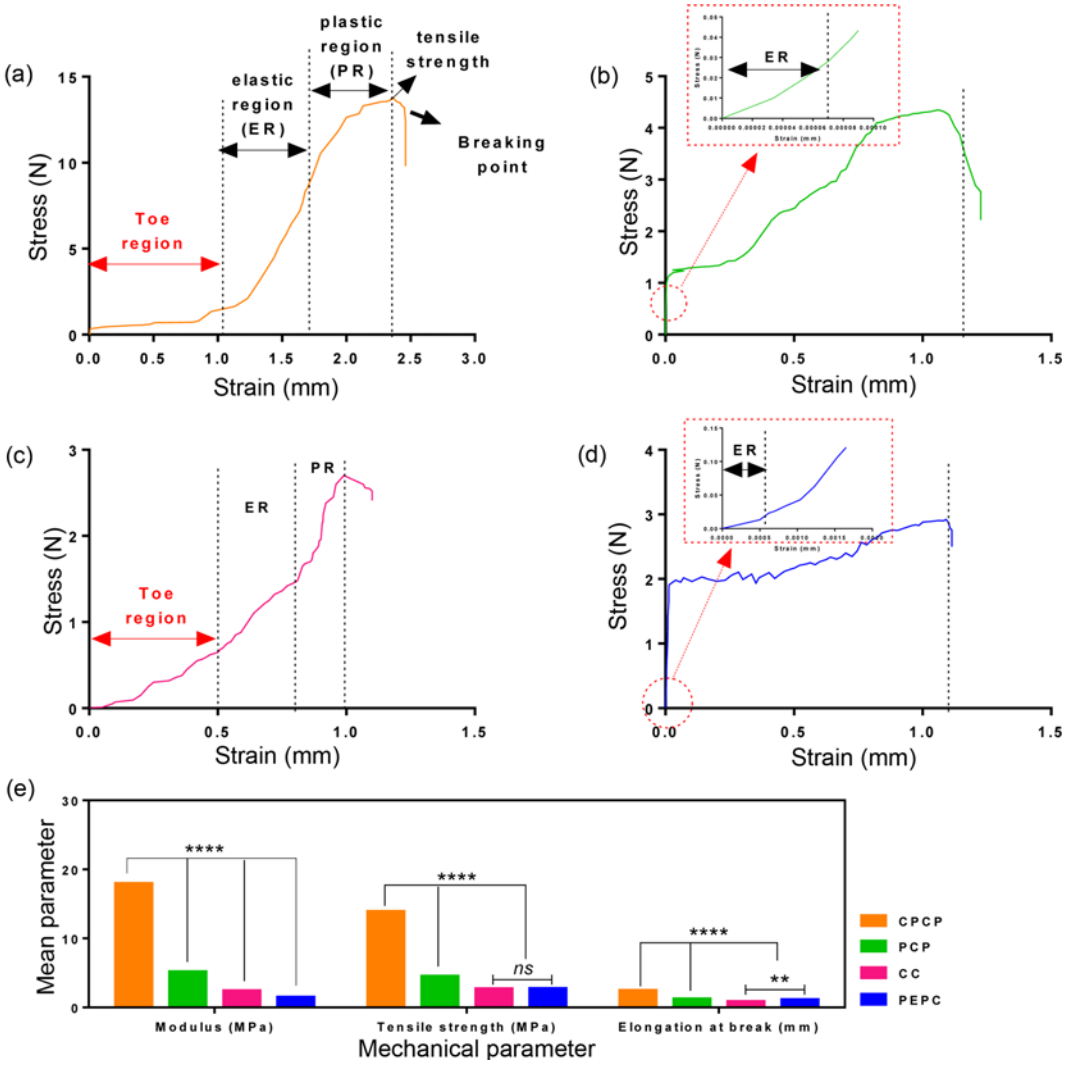

Figure 2. Stress-strain curve of the scaffolds; (a) CPCP, (b) PCP, (c) CC, (d) PEPC, and (e) the mechanical behavior of scaffolds (modulus, tensile strength, and elongation at break); ****: $p<0.001$; **: $p<0.05$.

Table 3. Mechanical parameters for all scaffolds and human dermis

Scaffolds code	Average elastic modulus (MPa)	Average tensile strength (MPa)	Average elongation at break (mm)
CPCP	17.9±0.22[b]	13.8±0.24[c]	2.4±0.06[a]
PCP	5.1±0.09[a]	4.4±0.19[a]	1.2±0.00[a]
CC	2.3±0.03[a]	2.6±0.07[b]	0.8±0.41[d]
PEPC	1.4±0.05[a]	2.7±0.22[b]	1.1±0.00[d]
DDM*	21.1±0.26[b]	13.7±0.26[c]	-

*Decellularized dermis matrix in the same study [51], [a]the mean difference is significant at the 0.001 level, [b]there is no significant difference between scaffolds (p>0.001), [c]there is no significant difference between scaffolds (p>0.05), [d]the mean difference is significant at the 0.05 level.

significant difference in mechanical strength between CPCP scaffold and DDM sample (p>0.05, Table 3) [51]. While some studies have reported lower mechanical properties of CPCP and DDM [52-54]. It seems that the skin location in the body plays a crucial role in this field. However, there are many reports that indicate reports higher modulus lead to much more cell adhesion, proliferation and differentiation on the surface [55].

Physical Behavior Analysis

Water-scaffold Interactions

To understand water-scaffold interactions and wound exudate absorption capacity, WCA and swelling tests were performed for 3D scaffolds (Figure 3(a) and (b)). The results indicated that the scaffold containing synthetic polymers (PEPC) provided a WCA greater than 90° and lower swelling compared to natural and hybrid scaffolds. It can be due to intrinsic poor hydrophilicity nature of PCL and the lower -OH bands in the chemical structure of PEPC [56]. In contrast to PECP, the WCA for CC scaffold exhibited a reduction of 38 % that was related to the more -OH functional groups in CC scaffold network (Figure 1 confirms).

It was also found that the addition of chitosan into the PEPC have enhanced the wettability of PCP scaffold than PEPC. Although a minor difference was observed in WCA values between CC and PCP scaffolds (p>0.05, ns), however, CC scaffold possesses a swelling% less than PCP that can be due to the higher degradation rate. Based on the results of WCA, the CPCP scaffold presented the highest wettability and consequently the smaller contact angle. Furthermore, in contrast to the mentioned scaffold after 48 h, the swelling percentage for PCP, CC, and PEPC showed a reduction of ~3, 21 and 54, respectively (Table 4). These results confirm the WCA data (Figure 3(a)). The studies have indicated the scaffolds hydrophilicity that related to the chemical structure of polymers is a key factor to increase the initial adhesion of cell and improve cellular responses. Furthermore, the rate of cell spreading and differentiation depends on surface hydrophilicity [57,58]. Consequently, CPCP scaffold can play an important role in the enhancement of cell adhesion

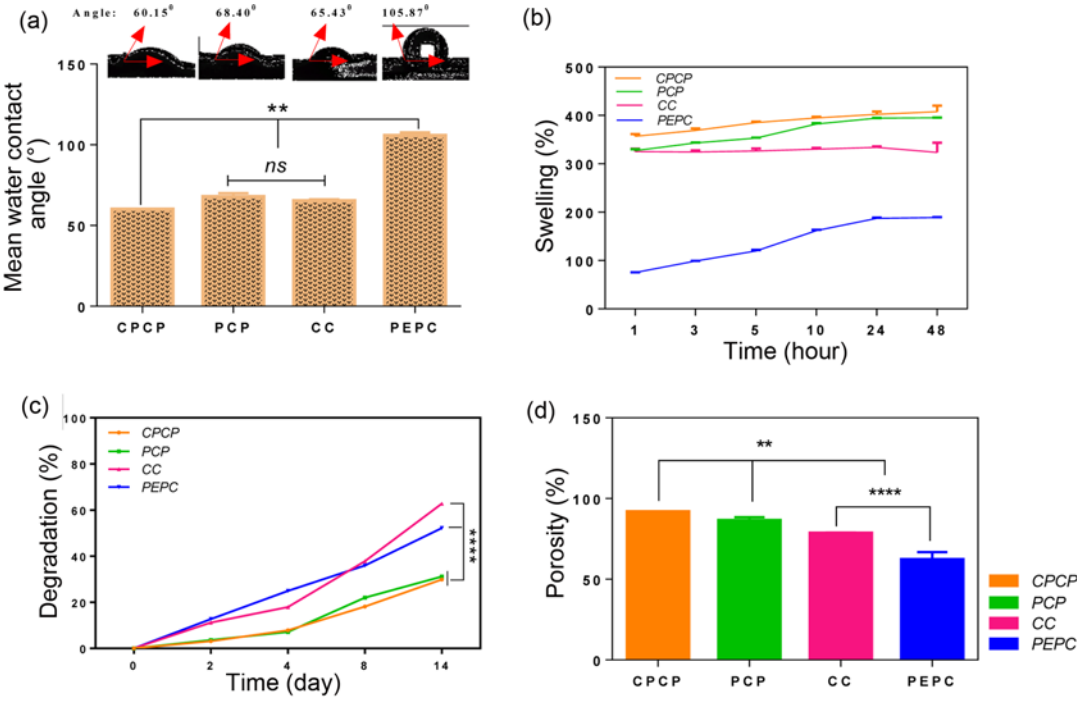

Figure 3. Physical behavior of scaffolds; (a) water contact angle, (b) swelling rate (during 48 h), (c) degradation rate (during 14 days), and (d) porosity. The (ns) is (no significant difference). **: p<0.05 and ****: p<0.001.

Table 4. Physical parameters of designed scaffolds

Scaffolds code	Swelling % at 48 h	Degradation % at day 14	Mean pore size (μm)	Porosity %
CPCP	407.57±12.52[a]	29.88±0.32[b]	53.74±27.33[b]	91.63±0.18[c]
PCP	395.14±0.66[a]	31.15±0.34[b]	86.43±26.09[b]	86.25±2.18[c]
CC	323.40±20.29[b]	62.77±0.25[b]	101.01±56.23[b]	78.49±0.44[b]
PEPC	189.03±0.95[b]	52.21±0.23[b]	104.92±62.47[b]	62.11±4.74[b]

[a]There is no significant difference between scaffolds ($p>0.001$), [b]the mean difference is significant at the 0.001 level, and [c]the mean difference is significant at the 0.05 level.

due to proper hydrophilicity, as well as act as a super-absorbent substrate/dressing for continuous absorption of wound exudates and wound healing management.

Degradation Analysis

The degradation rate of scaffolds was studied using lysozyme medium, for 14 days. The difference in the scaffolds degradation rate was illustrated in Figure 3(c). As the results show, natural and synthetic polymers-based scaffolds (i.e. PEPC and CC) had higher degradation% than hybrid scaffolds (i.e. CPCP and PCP) due to the presence of a large number of esters and amides groups that are susceptible to hydrolysis [59]. Nonetheless, the comparison of PEPC and CC degradation% demonstrated that the higher mass loss has recorded for the natural scaffold of CC (weight remaining less than 38 %). This can be explained by collagen-related peptide enzymatic hydrolysis. Although, the presence of collagen in the CPCP scaffold structure led to a decrease in degradation% (~4 %) relative to PCP which results in an increase of the available surface for cells proliferation and differentiation (Table 4). This could be due to better interactions and stronger intermolecular forces between collagen molecules and other polymers.

Porosity Study of Scaffolds

The reports have shown that intermolecular interactions can also provide porous microenvironment and improve cell-cell and cell-scaffold interactions [55]. The comparison of FTIR and porosity results confirmed the mentioned reports. As shown in Table 4, the higher porosity was recorded for CPCP scaffold. Indeed, the presence of the more amine, amide, and hydroxyl functional groups into CPCP scaffold structure was led to better interactions of polymer-polymer, the formation of new mini-bands and consequently a more porous structure (more than 90 %) compared to other scaffolds ($p<0.05$, Figure 3(d)). It is notable that, a significant decrease (~21 %) was observed in the porosity (%) of the PEPC scaffold compared to CC, due to the decrease of amine and amide functional groups ($p<0.001$). As a consequence, it was found that natural polymers play an important role in the porosity of scaffolds due to their functional groups.

Morphology of Scaffold and Cellular Adhesion

One of the main characterizes of skin engineered scaffolds is the morphological similarity to dermal-ECM. The structure of micro-porous along with uniform distribution increases the scaffold ability for cell proliferation and differentiation [60]. Selection of polymeric materials can play a crucial role in this field [61-63]. Additionally, the freezing temperature and the number of its steps can improve morphology, and size of ice crystals which in turn leads to control the pore size and porosity of 3D scaffold. Here, a two-stages freezing process was considered and the temperature of -20 °C as the initial freezing temperature was selected. Because supercooled temperatures range (to form ice crystals) is from -10 °C to -20 °C with ice nucleation typically occurring at -15 °C [33]. Therefore, the water molecules into polymer solutions gradually became solid and the ice crystals form by decreasing temperature from 0 to -4 °C, but a fast decrease of the temperature below -4 °C (-20 °C) results in stronger hydrogen bonding formation that leads to the control of degradation rate and creation of a denser scaffold with smaller pores size. With the growth of the ice nuclei, the polymer solution surrounding the ice nucleus was condensed and the chain segments of the macromolecules (such as collagen and chitosan) in the solution were close to each other and aggregated. It is notable that, in this stage, the temperatures below -20 °C result in the larger the temperature gradient, the longer the growth time of ice crystal and a heterogeneous structure for the scaffold. After 12 h, samples were held at a lower temperature (-80 °C as the secondary freezing temperature) to ensure that all the samples froze completely. Additionally, freezing at -80 °C, can help removal of the temperature gradient when ice crystals are sublimated by lyophilization (at -80 °C) and consequently the creation of a more stable structure. Finally, to understand the role of surfaces morphology in cell adhesion to scaffolds, the microstructures of the 3D scaffolds were evaluated using SEM analysis (Figure 4). As SEM images show, a combination of natural and synthetic polymers created an interconnected porous network along with the smaller pores size (Figure 4(a-d), Table 4). However, according to results of WAC and swelling, the presence of both of collagen and chitosan in the CPCP structure was led to the higher accumulation of amine and hydroxyl bands which results in the more ice crystals together with the aggregation of the collagen molecules into the interstitial spaces, during the fast freezing of CPCP hybrid solution, compared to PCP [33]. In followed by, sublimation process (removal of water from the frozen polymeric solution) in the freeze-drying method [64] led to the smaller pores diameter and the more uniform distribution of size and consequently greater cell adhesion and spreading on the scaffold (Figure 4(e-h)). Therefore, the larger diameter of pores in PEPC scaffold are related to hydrophobic groups of PCL and contact angle higher than 90 ° (between the surface

and biological fluids) that avoid cellular adhesion and distribution. Moreover, the difference in the mean pores size and cellular adhesion between CPCP and CC scaffolds can be due to better interactions of collagen with PCL. The histogram of pores size based on normal distribution curve (black line) showed a smoother curve for the CPCP scaffold than PCP, CC and PEPC (Figure 4(i-l)).

Consequently, it is notable that functional groups (amide, amine, and hydroxyl) played an important impact on the decrease of pores size and subsequent cell-scaffold adhesion. The SEM images of cell adhesion confirm the mentioned results (Figure 4(e-h)). It has shown that polymeric materials can present a wide range of pore size in skin tissue engineering applications. Accordingly, pore sizes ranging from 5 to 337 μm have been suggested for skin regeneration [21,63,65,66] although, pores diameter in the range of 15 to 160 μm are ideal [62,67-71].

Cell Viability, Proliferation, and Differentiation

The biocompatibility and HSF cells viability onto the scaffolds was assayed by MTT analysis, during 24, 48, and 72 h. As shown in Figure 5(a), all scaffolds were nontoxic however highest cell viability% was observed on CPCP scaffold (~98 %), and there was no significant difference between CPCP scaffold and control group at each individual time point ($p>0.001$). This could be due to the higher porosity and wettability (WCA=60 °) in the of CPCP structure, that results in the increase of cellular proliferation than other groups, after 72 h (Figure 5(b)). The various studies confirm that cells spreading, proliferation and differentiation increases when the contact angle of water with the surface is between 60 ° and 80 ° [55,72-74]. Thus, PEPC scaffold revealed the lowest cell viability% among groups studied ($p<0.001$). Further, evaluation of data indicated that cell viability and proliferation on the CC and PCP scaffolds was led to a ~11 % and 2 % decrease respectively, compared to CPCP, due to higher degradation rate. It is notable that there were no cellular morphological changes during the course of the incubation period (72 h).

In followed by, RT-PCR analysis was performed to evaluate 3D scaffolds potential for wound healing (in vitro), via studying keratinocytes proliferation and differentiation from h-ASCs, after 7 and 14 days. Because keratinocytes are found in various layers of skin and play an important role in the integrity and re-epithelialization of skin [75]. In this field, most important keratinocytes include keratinocytes 14,

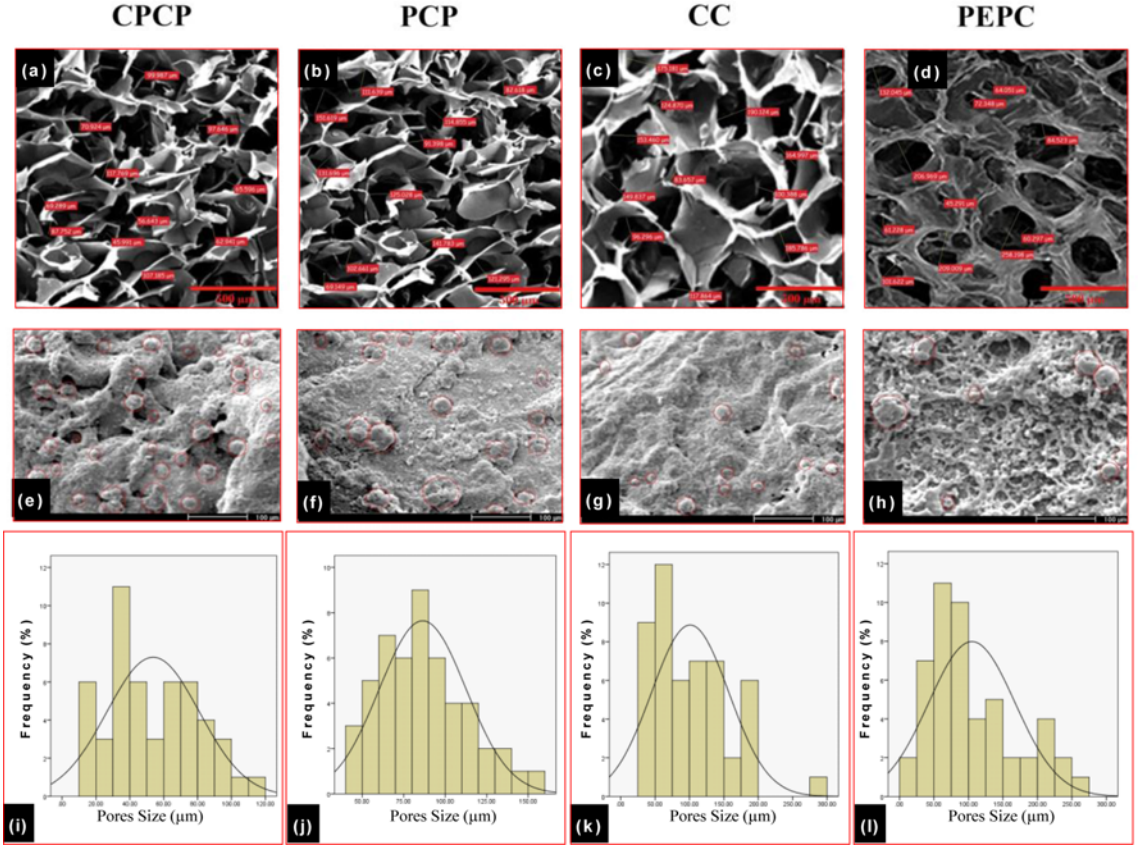

Figure 4. Morphology of scaffolds; (a-d) before the seeding cells, (e-h) After the seeding cells, (i-h) Histograms of pores size based on normal distribution curve (black line).

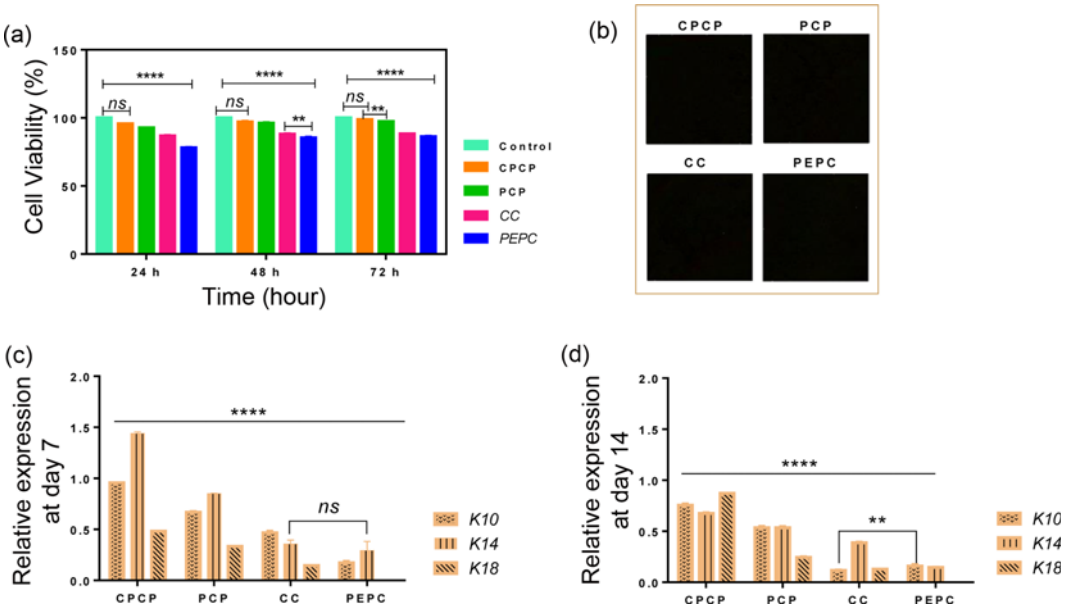

Figure 5. (a) The viability of HSF cells cultured on all four scaffolds (during 24, 48 and 72 h), (b) the inverted microscope images of HSF cells distribution and proliferation on the scaffolds, (c) expression of K10 and K14 on the scaffolds at day 7, and (d) expression of K10 and K14 on the scaffolds at day 14. The (ns) and (****) and (**) are defined as no significant difference, $p<0.001$ and $p<0.05$.

10 and 18 (K14, K10, and K18) which are expressed in basal and suprabasal layers (in the epidermis), and internal secretory/embryonic epithelial cells such as hair follicle, sweat/sebaceous glands (in the dermis), respectively [76-79]. An ideal skin-engineered scaffold not only should induce the mentioned keratinocytes but also imitate differentiation pattern, because mimicking how to express keratinocytes on the scaffold (expression of early or late) is effective in the speed up wound healing.

Our results showed that the selection of polymers plays an important role in mimicking keratinocytes differentiation pattern. Such that, the higher expression level of keratinocytes was observed for CPCP scaffold Figure 5(c) and (d)). Moreover, evaluation of the differentiation pattern showed that the mentioned scaffold has been imitated a pattern similar to epidermis and dermis for inducing K10, K14, and K18. It is notable that, K10 and K14 have known as early differentiation markers at day 7 [80] and K18 is as late differentiation marker that its expression peak occurs after 7 days [79]. It was found that the lowest gene expression level after 14 days was related to CC scaffold due to higher degradation rate and lower modulus ($p<0.001$). Notably, K18 was not induced on the PEPC due to low modulus, WCA and porosity.

Our study clearly indicated that expression of keratinocytes (K14 and K10 and K18) and their growth pattern on the scaffold was directly correlated with hydrophobicity, modulus, and structure of scaffold (Figure 5(c) and (d)). As a result, CPCP 3D-scaffold can potentially enhance h-ASCs differentiation into keratinocytes (without growth factor) and lead to the regeneration of both epidermis and dermis layers by mimicking the cellular proliferation and differentiation.

Conclusion

In this study, we successfully designed a hybrid 3D-scaffold that can potentially induce keratinocytes (in the absence of growth factor) and accelerate the wound healing process. This scaffold titled as abbreviation CPCP includes the natural polymers of collagen and chitosan modified PEG and PCL that possess the chemical structure similar to macromolecules of the extracellular matrix such as polysaccharide chains (glycosaminoglycans (GAGs)) and fibrous proteins. The mentioned scaffold, along with three other scaffolds (CC, PEPC, and PCP) were evaluated by means of FTIR, tensile, water contact angle, SEM as well as swelling, degradation rate, and porosity (%) assays, to determine the role of polymers in the cell behavior (adhesion, proliferation, viability, and differentiation) and compare the physicochemical, biomechanical and structural similarities to the skin. The surface chemistry and elasticity analysis showed that the CPCP scaffold possesses more similar to native human skin (irrespective from skin location in the body) compared to other scaffolds. Comparison of data also showed that CPCP scaffold provided an interconnected porous network with the proper pores size for fibroblast cells proliferation. The swelling and degradation rate showed that the mentioned scaffold can act as the substrate/dressing for continuous absorption of wound exudates. Furthermore, it

was found that CPCP can promote not only human skin fibroblast cells adhesion and proliferation, but also differentiate h-ASCs into both keratinocytes of epidermis and dermis, by mimicking human keratinocytes differentiation pattern. It is due to biocompatibility, hydrophilicity, and the structural similarity of the CPCP network to the macromolecular-based components of the ECM. The results show how to select and combine polymers play a crucial impact on scaffold behavior for wound healing. As a consequence, CPCP can be used as a substrate or dressing in tissue engineering application for skin regeneration.

Acknowledgments

We would like to express our deep appreciation to Dr. Arash Sarveazad for all his guidance that has given us over the past three years.

References

1. A. I. Aghmiuni and A. A. Khiavi in "Aromatic and Medicinal Plants - Back to Nature" (H. A. El-Shemy Ed.), pp.1-28, InTech, Rijeka, https://doi.org/10.5772/67062, 2017.
2. C. Harvey, *Orthop. Nurs.*, **24**, 143 (2005).
3. A. S. Halim, T. L. Khoo, and S. J. Mohd Yussof, *Indian J. Plast. Surg. Off. Publ. Assoc. Plast. Surg. India*, **43**, S23 (2010).
4. I. Brockmann, J. Ehrenpfordt, T. Sturmheit, M. Brandenburger, C. Kruse, M. Zille, D. Rose, and J. Boltze, *Stem Cells Int.*, **2018**, 1 (2018).
5. Ö. S. Somuncu, C. Karahan, S. Somuncu, and F. Şahin in "Stem Cells in Clinical Practice and Tissue Engineering", (R. Sharma Ed.), pp.315-333, IntechOpen, Rijeka, https://doi.org/10.5772/intechopen.69905, 2018.
6. K. Vig, A. Chaudhari, S. Tripathi, S. Dixit, R. Sahu, S. Pillai, V. Dennis, and S. Singh, *Int. J. Mol. Sci.*, **18**, 789 (2017).
7. N. Bhardwaj, D. Chouhan, and B. B. Mandal, *Curr. Pharm. Des.*, **23**, 3455 (2017).
8. C. Pang, A. Ibrahim, N. W. Bulstrode, and P. Ferretti, *Int. Wound J.*, **14**, 450 (2017).
9. N. Sultana in "Functional 3D Tissue Engineering Scaffolds" (Y. Deng and J. Kuiper Eds.), pp.1-21, Woodhead Publishing, http://www.sciencedirect.com/science/article/pii/B978008100979600001X, 2018.
10. V. Andreu, G. Mendoza, M. Arruebo, and S. Irusta, *Materials (Basel)*, **8**, 5154 (2015).
11. Y. Xu, D. Xia, J. Han, S. Yuan, H. Lin, and C. Zhao, *Carbohydr. Polym.*, doi:10.1016/j.carbpol.2017.08.069 (2017).
12. F. Khan and S. R. Ahmad, *Macromol. Biosci.*, **13**, 395 (2013).
13. S. Ahmed and S. Ikram, *Achiev. Life Sci.*, **10**, 27 (2016).
14. S. Ahmed and M. Ahmad, *Immunochem. Immunopathol.*, **1**, 2 (2015).
15. R. Zhao, X. Li, B. Sun, Y. Zhang, D. Zhang, Z. Tang, X. Chen, and C. Wang, *Int. J. Biol. Macromol.*, **68**, 92 (2014).
16. N. Cai, C. Li, C. Han, X. Luo, L. Shen, Y. Xue, and F. Yu, *Appl. Surf. Sci.*, **369**, 492 (2016).
17. M. Mori, S. Rossi, F. Ferrari, M. C. Bonferoni, G. Sandri, T. Chlapanidas, M. L. Torre, and C. Caramella, *J. Pharm. Sci.*, **105**, 1180 (2016).
18. B. H. León-Mancilla, M. A. Araiza-Téllez, J. O. Flores-Flores, and M. C. Piña-Barba, *J. Appl. Res. Technol.*, **14**, 77 (2016).
19. M. Rodríguez-Vázquez, B. Vega-Ruiz, R. Ramos-Zúñiga, D. A. Saldaña-Koppel, and L. F. Quiñones-Olvera, *Biomed Res. Int.*, **2015**, 1 (2015).
20. G. Kim, S. Ahn, Y. Kim, Y. Cho, and W. Chun, *J. Mater. Chem.*, **21**, 6165 (2011).
21. L. Ma, C. Gao, Z. Mao, J. Zhou, J. Shen, X. Hu, and C. Han, *Biomaterials*, **24**, 4833 (2003).
22. C. Tangsadthakun, S. Kanokpanont, N. Sanchavanakit, T. Banaprasert, and S. Damrongsakkul, *J. Met. Mater. Miner.*, **16**, 37 (2006).
23. D. Indrani, F. Lukitowati, and Y. Yulizar, *IOP Conf. Ser. Mater. Sci. Eng.*, **202**, 12020 (2017).
24. V. T. Tchemtchoua, G. Atanasova, A. Aqil, P. Filée, N. Garbacki, O. Vanhooteghem, C. Deroanne, A. Noël, C. Jérome, B. Nusgens, Y. Poumay, and A. Colige, *Biomacromolecules*, **12**, 3194 (2011).
25. Y. Yan, X. Zhang, C. Li, Y. Huang, Q. Ding, and X. Pang, *Appl. Surf. Sci.*, **332**, 62 (2015).
26. G. BaoLin and P. X. Ma, *Sci. China. Chem.*, **57**, 490 (2014).
27. B. Dhandayuthapani, Y. Yoshida, T. Maekawa, and D. S. Kumar, *Int. J. Polym. Sci.*, **2011**, doi:10.1155/2011/290602 (2011).
28. M. Mir, M. N. Ali, A. Barakullah, A. Gulzar, M. Arshad, S. Fatima, and M. Asad, *Prog. Biomater.*, **7**, 1 (2018).
29. S.-H. Chen, C.-T. Tsao, C.-H. Chang, Y.-T. Lai, M.-F. Wu, C.-N. Chuang, H.-C. Chou, C.-K. Wang, and K.-H. Hsieh, *Mater. Sci. Eng. C*, **33**, 2584 (2013).
30. S. Eshraghi and S. Das, *Acta Biomater.*, **6**, 2467 (2010).
31. K. T. Shalumon, K. H. Anulekha, K. P. Chennazhi, H. Tamura, S. V. Nair, and R. Jayakumar, *Int. J. Biol. Macromol.*, **48**, 571 (2011).
32. Y. Wu and Y. Han in "Functional 3D Tissue Engineering Scaffolds", pp.367-390, Elsevier, http://dx.doi.org/10.1016/B978-0-08-100979-6.00014-8, 2017.
33. Z. Fereshteh in "Functional 3D Tissue Engineering Scaffolds" (Y. Deng and J. Kuiper Eds.), pp.151-174, Elsevier, http://www.sciencedirect.com/science/article/pii/B9780081009796000070), 2018.
34. S. P. Huang, C. C. Hsu, S. C. Chang, C. H. Wang, S. C. Deng, N. T. Dai, T. M. Chen, J. Y. H. Chan, S. G. Chen, and S. M. Huang, *Ann. Plast. Surg.*, **69**, 656 (2012).
35. W. K. Ong and S. Sugii, *Int. J. Biochem. Cell Biol.*, **45**, 1083 (2013).
36. R. Dai, Z. Wang, R. Samanipour, K. Koo, and K. Kim,

Stem Cells Int., **2016**, 1 (2016).
37. L. Frese, P. E. Dijkman, and S. P. Hoerstrup, *Transfus. Med. Hemotherapy*, **43**, 268 (2016).
38. available at https://www.astm.org/DATABASE.CART/HISTORICAL/D3039D3039M-00.htm.
39. U. J. Kim, J. Park, H. Joo Kim, M. Wada, and D. L. Kaplan, *Biomaterials*, **26**, 2775 (2005).
40. K. K. Nayak and P. Gupta, *Int. J. Biol. Macromol.*, **81**, 1 (2015).
41. S. Miguel, M. Ribeiro, P. Coutinho, and I. Correia, *Polymers (Basel)*, **9**, 183 (2017).
42. S. Heidari Keshel, M. Rostampour, G. Khosropour, B. A. Bandbon, A. Baradaran-Rafii, and E. Biazar, *J. Biomater. Sci. Polym. Ed.*, **27**, 339 (2015).
43. S. S. Sarvandi, M. T. Joghataei, K. Parivar, M. Khosravi, A. Sarveazad, and N. Sanadgol, *Iran. J. Basic Med. Sci.*, **18**, 89 (2015).
44. P. Thevenot, W. Hu, and L. Tang, *Curr. Top. Med. Chem.*, **8**, 270 (2008).
45. B. G. Keselowsky, D. M. Collard, and A. J. Garcia, *J. Biomed. Mater. Res. A*, **66**, 247 (2003).
46. T. Riaz, R. Zeeshan, F. Zarif, K. Ilyas, N. Muhammad, S. Z. Safi, A. Rahim, S. A. A. Rizvi, and I. U. Rehman, *Appl. Spectrosc. Rev.*, **53**, 703 (2018).
47. F. Selmin, F. Cilurzo, A. Aluigi, S. Franzè, and P. Minghetti, *Results Pharma Sci.*, **2**, 72 (2012).
48. D. M. Mackie in Sensing Technologies for Global Health, Military Medicine, Disaster Response, and Environmental Monitoring II; and Biometric Technology for Human Identification IX, Vol. 8371, pp.83711T-83711T-8 (2012).
49. G. Ahn, K. H. Min, C. Kim, J. S. Lee, D. Kang, J. Y. Won, D. W. Cho, J. Y. Kim, S. Jin, W. S. Yun, and J. H. Shim, *Sci. Rep.*, **7**, 1 (2017).
50. N. I. Afanasyeva, *Macromol. Symp.*, **141**, 117 (1999).
51. P. B. Milan, N. Lotfibakhshaiesh, M. T. Joghataie, J. Ai, A. Pazouki, D. L. Kaplan, S. Kargozar, N. Amini, M. R. Hamblin, M. Mozafari, and A. Samadikuchaksaraei, *Acta Biomater.*, **45**, 234 (2016).
52. C. M. Healy and J. G. Boorman, *Burns. Incl. Therm. Inj.*, **15**, 52 (1989).
53. T. M. MacLeod, A. Cambrey, G. Williams, R. Sanders, and C. J. Green, *Burns*, **34**, 1169 (2008).
54. M. Vitacolonna, M. Mularczyk, F. Herrle, T. J. Schulze, H. Haupt, M. Oechsner, L. R. Pilz, P. Hohenberger, and E. D. Rössner, *BMC Surg.*, **14**, 7 (2014).
55. H.-I. Chang and Y. Wang in "Regenerative Medicine and Tissue Engineering - Cells and Biomaterials", Vol. 2, p.64, http://www.intechopen.com/books/genetic-engineering-basics-new-applications-and-responsibilities/gateway-vectors-for-plant-genetic-engineering-overview-of-plant-vectors-application-for-bimolecular-), InTech, 2011.
56. S. Moeini, M. R. Mohammadi, and A. Simchi, *Bioact. Mater.*, **2**, 146 (2017).
57. J. M. Goddard and J. H. Hotchkiss, *Prog. Polym. Sci.*, **32**, 698 (2007).
58. L.-C. Xu and C. A. Siedlecki, *Biomaterials*, **28**, 3273 (2007).
59. T. Snape, Astles. Alison, J. Davies, A. Astles, and J. Davies, *Pharm. J.*, **385**, 416 (2010).
60. S. H. Keshel, M. Soleimani, M. R. Tavirani, M. Ebrahimi, R. Raeisossadati, H. Yasaei, D. Afsharzadeh, M. J. Behroz, A. Atashi, S. Amanpour, A. Khoshzaban, R. Roozafzoon, and G. R. Behrouzi, *Mol. Reprod. Dev.*, **79**, 709 (2012).
61. M. Kim and G. Kim, *RSC Adv.*, **5**, 26954 (2015).
62. D. E. López Angulo and P. J. do Amaral Sobral, *Int. J. Biol. Macromol.*, **92**, 645 (2016).
63. T. W. Wang, H. C. Wu, Y. C. Huang, J. S. Sun, and F. H. Lin, *Artif. Organs*, **30**, 141 (2006).
64. E. Sachlos, J. T. Czernuszka, S. Gogolewski, and M. Dalby, *Eur. Cells Mater.*, **5**, 29 (2003).
65. X. Zhu, W. Cui, X. Li, and Y. Jin, *Biomacromolecules*, **9**, 1795 (2008).
66. D. Atila, D. Keskin, and A. Tezcaner, *Carbohydr. Polym.*, **133**, 251 (2015).
67. F. J. O'Brien, B. A. Harley, I. V. Yannas, and L. J. Gibson, *Biomaterials*, **26**, 433 (2005).
68. J. Ma, H. Wang, B. He, and J. Chen, *Biomaterials*, **22**, 331 (2001).
69. W. F. Lee and Y. J. Chen, *J. Appl. Polym. Sci.*, **82**, 2487 (2001).
70. J. Yang, G. Shi, J. Bei, S. Wang, Y. Cao, Q. Shang, G. Yang, and W. Wang, *J. Biomed. Mater. Res.*, **62**, 438 (2002).
71. H.-I. Chang and Y. Wang in *Regenerative Medicine and Tissue Engineering - Cells and Biomaterials*, 2011.
72. J. Wei, T. Igarashi, N. Okumori, T. Igarashi, T. Maetani, B. Liu, and M. Yoshinari, *Biomed. Mater.*, **4**, 45002 (2009).
73. D. Dowling, I. Miller, M. Ardhaoui, and W. Gallagher, *J. Biomater. Appl.*, **26**, 327 (2011).
74. E. D. Yildirim, R. Besunder, D. Pappas, F. Allen, S. Güçeri, and W. Sun, *Biofabrication*, **2**, 14109 (2010).
75. C. Reshmi, P. Suja, O. Manaf, P. Sanu, and A. Sujith, *Int. J. Biol. Macromol.*, **108**, 1261 (2018).
76. R. Moll, M. Divo, and L. Langbein, *Histochem. Cell Biol.*, **129**, 705 (2008).
77. L. Cassimeris, G. Plopper, and V. R. Lingappa, "Lewin's CELLS", Jones & Bartlett Learning, LLC, 2011; https://books.google.com/books?id=wHxomxPuWYkC.
78. G. Guasch, *Biol. Eng. Stem Cell Niches*, 127-143 (2017).
79. A. M. B. Tadeu and V. Horsley, "Epithelial Stem Cells in Adult Skin", Vol. 107, http://dx.doi.org/10.1016/B978-0-12-416022-4.00004-4), Elsevier Inc., ed. 1, 2014.
80. E. B. Lane and W. H. I. McLean, *J. Pathol.*, **204**, 355 (2004).